

Weight Effects on the Periodic Ambiguity Function

BENJAMIN GETZ
NADAV LEVANON
Tel-Aviv University

CW radar signals and processors are discussed. The use of the periodic ambiguity function (PAF) to analyze the delay-Doppler performance of CW signals and their corresponding correlation receivers, is extended to include weight function effects. This work provides tools which can predict the delay-Doppler response of almost any phase-coded CW radar. Examples demonstrate that a combination of CW signals having perfect periodic autocorrelation, a matched reference signal with a large number of modulation periods and a smooth weight function, can create a delay-Doppler response with extremely low sidelobes, strongly resembling the response of a coherent pulse train.

Manuscript received August 10, 1992; revised June 3, 1993.

IEEE Log No. T-AES/31/1/07981.

Authors' address: Dept. of Electrical Engineering-Systems, Tel-Aviv University, Tel-Aviv, 69978, Israel.

0018-9251/95/\$4.00 © 1995 IEEE

I. INTRODUCTION

Periodically modulated CW signals can be considered as the ultimate in pulse compression. They achieve a unity peak-to-average power ratio. They can also exhibit an ideal (zero) range sidelobes on the zero-Doppler axis, a property which eludes pulse compression signals. CW signals have other properties, such as low probability of intercept when observed by conventional electronic support measures. These advantages make CW an important and viable radar concept.

The ideal (zero) range sidelobes properties of CW signals can be reached when the signal exhibits perfect periodic autocorrelation, and the correlation receiver is matched to an integral number of modulation periods. The delay-Doppler response of such a system can be predicted by the periodic ambiguity function (PAF) [1]. However, off the delay axis, there are Doppler sidelobes. As in a coherent-pulse-train radar, Doppler sidelobes in a CW radar can be suppressed by a weight function in the receiver. The discussion in [1] is extended here to include the effect of a weight function on the delay-Doppler response of CW radar signals. In particular we are concerned with the effect of nonuniform weight function on the property of perfect periodic autocorrelation. Should the weight function be a smooth one, changing within the modulation period, or should it change in steps of a duration equal to the modulation period? In order to answer these questions we use a combination of theoretical analysis and computational examples. We show that contrary to our initial intuition [2], a smooth rather than staircase weight function should be preferred.

Short of the effects of hardware imperfections, we provide tools for predicting the delay-Doppler response of any phase-coded CW radar, in which an integer number of modulation periods are processed. The analysis is limited to phase-coded signals because they can yield better response than frequency modulated CW signals, and because FM signals can be approximated by phase-coded signals. Our examples include the Kretschmer and Lewis P3 and P4 signals [3], which are related to linear-FM, but exhibit the property of perfect periodic autocorrelation, not shared by linear-FM. We show that P signals yield a delay-Doppler response which is the closest (among CW signals) to the response obtained by a coherent pulse train. We also demonstrate the somewhat different delay-Doppler response obtained by the two-valued signals, suggested recently by Bomer and Antweiler [4] and independently by Golomb [5]. Finally we examine the behavior of Ipatov's [6] binary signals (0° and 180°) which exhibit perfect periodic *crosscorrelation* with a slightly mismatched reference signal.

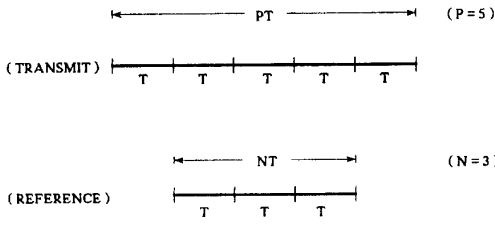


Fig. 1. Relative durations of transmitted and reference signals.

II. PERIODIC AMBIGUITY FUNCTION

The PAF serves CW radar signals, in a similar role to which the well known ambiguity function serves finite duration signals. The regular ambiguity function describes the delay-Doppler response of a matched receiver. The matched receiver is a correlation receiver in which the reference signal is of *exactly* the same duration as the finite duration signal.

Due to finite target dwell time, CW signals are also of finite duration. We consider a periodically modulated radar signal of duration PT , where T is the modulation period and $P > 1$. The return signal is received by a correlation-type receiver, containing a reference signal which is the conjugate of N (an integer) periods of the transmitted signal, with $N < P$, as demonstrated in Fig. 1. In other words, the receiver is matched to N periods of the signal. Within the duration of the signal, the periodicity implies that the complex envelope of the transmitted signal $u(t)$ obeys

$$u(t) = u(t + nT), \quad n = 0, \pm 1, \pm 2, \dots \quad (1)$$

As long as the delay τ is shorter than the difference between the dwell time and the length of the reference signal, $0 \leq \tau \leq (P - N)T$, the output response of such a receiver, in the delay-Doppler plane, is given by the PAF

$$|\chi_{NT}(\tau, \nu)| = \frac{1}{NT} \left| \int_0^{NT} u(t - \tau) u^*(t) \exp(j2\pi\nu t) dt \right| \quad (2)$$

where τ is assumed to be a constant and the delay rate of change is represented by the Doppler shift ν .

The PAF was discussed in [1] where it was written in a slightly different way involving $u(t + \tau/2)u^*(t - \tau/2)$. The format in [1] yields symmetry with respect to the origin, but a periodicity of $2T$, while the format in (2) results in a PAF which is not symmetrical but which has a periodicity of T . The subtle differences are discussed in a different paper [7]. The format in (2) requires a more simple receiver implementation. The conclusions are generally not affected by the different formats, including the interesting property, proved in [1], that the PAF for N periods, is related to the single-period ambiguity function, by a universal

relationship

$$|\chi_{NT}(\tau, \nu)| = |\chi_T(\tau, \nu)| \left| \frac{\sin(N\pi\nu T)}{N \sin(\pi\nu T)} \right| \quad (3)$$

where

$$|\chi_T(\tau, \nu)| = \frac{1}{T} \left| \int_0^T u(t - \tau) u^*(t) \exp(j2\pi\nu t) dt \right|. \quad (4)$$

The PAF applies to any kind of periodic modulation including pulses (amplitude modulation). However, we discuss only CW phase-modulated signals.

As pointed out in the Introduction, this paper generalizes the discussion in [1] by evaluating the delay-Doppler response for two practical modifications of the matched receiver. (1) The reference signal may be multiplied by a weight function. (2) The reference signal may be different from the (conjugate of) the transmitted signal. A general discussion of the new response appears in Section III.

III. DELAY-DOPPLER RESPONSE

The complex envelope $u(t)$ of the radar signal remains periodic as given in (1). The complex envelope of the reference signal $r(t)$ is also periodic with the same period T . The fact that the reference signal is limited in duration to NT is expressed by multiplying it with the rectangular window function

$$p(t) = \begin{cases} 1, & 0 \leq t \leq NT \\ 0, & \text{elsewhere} \end{cases} \quad (5)$$

The reference signal is also multiplied by a weight function $w(t)$. Of course there is no effect to the weight function outside the rectangular window of width NT . The response of a correlation receiver can now be described by the function

$$|\psi(\tau, \nu)| = \left| \int_{-\infty}^{\infty} u(t - \tau) r(t) p(t) w(t) \exp(j2\pi\nu t) dt \right|. \quad (6)$$

Equation (6) is effectively the Fourier transform (using negative sign before the frequency term) of two products, and can therefore be described by the convolution (denoted by \otimes) of two Fourier transforms,

$$|\psi(\tau, \nu)| = \left| \int_{-\infty}^{\infty} u(t - \tau) r(t) \exp(j2\pi\nu t) dt \otimes \int_{-\infty}^{\infty} p(t) w(t) \exp(j2\pi\nu t) dt \right|. \quad (7)$$

Regarding the first transform, since both $u(t)$ and $r(t)$ are infinitely long and periodic with period T , their product (for any τ) is also infinite and periodic with period T . It is well known that the Fourier transform

of such a periodic signal is a series of delta functions at $\nu = n/T$, $n = 0, \pm 1, \pm 2, \dots$. In Appendix A we show that

$$\begin{aligned} & \int_{-\infty}^{\infty} u(t - \tau)r(t) \exp(j2\pi\nu t) dt \\ &= \sum_{n=-\infty}^{\infty} \delta\left(n - \frac{n}{T}\right) g_n(\tau) \end{aligned} \quad (8)$$

where

$$g_n(\tau) \equiv \frac{1}{T} \int_0^T u(t - \tau)r(t) \exp\left(\frac{j2\pi n t}{T}\right) dt. \quad (9)$$

The second transform in (7) is the Fourier transform of the product of the rectangular window and the weight function, which are termed $W(\nu)$

$$\begin{aligned} W(\nu) &= \int_{-\infty}^{\infty} p(t)w(t) \exp(j2\pi\nu t) dt \\ &= \int_0^{NT} w(t) \exp(j2\pi\nu t) dt. \end{aligned} \quad (10)$$

The delay-Doppler response of the correlation receiver is obtained from the convolution between (8) and (10), yielding

$$|\psi(\tau, \nu)| = \left| \sum_{n=-\infty}^{\infty} g_n(\tau) W\left(\nu - \frac{n}{T}\right) \right|. \quad (11)$$

The approach taken in this section is similar to the approach used in [8, Section 8.3], for a weighted uniform pulse train. To proceed any further, we must define the complex envelopes of the transmitted signal $u(t)$ and the reference signal $r(t)$, in order to find $g_n(\tau)$, and we must also define the weight function in order to find $W(\nu)$. The fall-off rate of $W(\nu)$ determines how many terms of the infinite sum in (11) have a valuable contribution to the result.

IV. WEIGHT WINDOWS

We begin our discussion of weight function by choosing a smooth (no steps) weight function $w(t)$ across the entire duration of the reference signal. Three important and well known weight windows can be defined by selecting the parameter c in the following expression

$$\begin{aligned} p(t)w(t) &= \frac{1}{NT} \left(1 - \frac{1-c}{c} \cos \frac{2\pi t}{NT}\right), \\ &0 \leq t \leq NT, \quad \text{zero elsewhere.} \end{aligned} \quad (12)$$

For Uniform, Hann, and Hamming weight windows select $c = 1, 0.5$, and 0.53836 respectively. Performing the transform of the expression in (12) yields

$$W(\nu) = \frac{\sin(\pi\nu NT)}{\pi\nu NT} \left(1 + \frac{(1-c)(\nu NT)^2}{c[1-(\nu NT)^2]}\right) \exp(j\pi\nu NT). \quad (13)$$

When $(\nu NT)^2 = 1$, (13) yields $W(\nu) = -(1-c)/2c$. The exponent in (13) is due to the fact that the weight function is not centered about $t = 0$. The transform for a centered window can be found in many references, for example in [9].

With these examples of $W(\nu)$ we can comment on the meaning of (11). More specifically, which terms of the sum over n are significant. For example, when calculating the response at the delay axis, namely at $\nu = 0$, we obviously need $g_0(\tau)$ since it is multiplied by a weight of $W(0) = 1$. To this we must add the value of $g_1(\tau)$ multiplied by $W(1/T)$ because the weight function is now centered at $\nu = 1/T$. For the family of weight windows to which (13) applies, when N is an integer, $W(\nu = 1/T)$ is always zero. More generally

$$W\left(\frac{n}{T}\right) = 0, \quad n = \pm 1, \pm 2, \dots \quad (14)$$

Equation (14) implies that there is no contribution of $g_n(\tau)$ at $\nu = 0$ when $n \neq 0$. The ν nearest to zero, where the contribution of $g_1(\tau)$ peaks for the first time, is at $\nu = 1/2NT$. There $g_1(\tau)$ is multiplied by the peak of the N th sidelobe of $W(\nu)$, which is, for Hann, $10 + 60\log(N)$ dB down. The contribution of the $n = 2$ term is attenuated according to the level of the $2N$ th sidelobe of $W(\nu)$, which for Hann is $10 + 60\log(2N)$ dB, etc.. For $N = 16$, the relative effects of the $n = 0, 1$ and 2 terms are: 0 dB, -82 dB and -100 dB, respectively. For this case (Hann, $N = 16$), for $|\nu| < 1/T$, it will usually suffice to use only the $n = 0, \pm 1$ and ± 2 terms of the sum in (11).

Still missing from the analysis is the $g_n(\tau)$ function defined in (9). We are interested in periodic CW signals (or pair of signals) which exhibit perfect periodic autocorrelation (or cross-correlation). We limit the discussion to three examples of phase-coded signals. From the matched polyphase codes we use the Lewis and Kretschmer P3 and P4 signals [3], from the matched two-phase codes we use a code discussed by Bomer and Antweiler [4] and by Golomb [5], and the last signal belongs to the family of unmatched pairs as discussed by Ipatov and Fedorov [6].

V. PHASE-CODED CW PERIODIC SIGNALS

The period of the modulation signal is divided into M bits, each of duration t_b

$$T = Mt_b \quad (15)$$

with

$$u(t) = \sum_{m=1}^M u_m[t - (m-1)t_b], \quad 0 \leq t \leq T. \quad (16)$$

For $t > T$ or $t < 0$ use (1). The bits are phase modulated by the phase sequence $\{\phi_m\}$ of length M ,

$$u_m(t) = \begin{cases} \exp(j\phi_m), & 0 \leq t \leq t_b \\ 0, & \text{elsewhere} \end{cases} \quad (17)$$

In order to be able to handle Ipatov's pairs of signals as well, we generalize the reference signal in the receiver and allow amplitude differences. Hence, the bits of the reference signal $r_m(t)$ are not just the conjugates of $u_m(t)$ but are

$$r_m(t) = \begin{cases} b_m \exp(-j\phi_m), & 0 \leq t \leq t_b \\ 0, & \text{elsewhere} \end{cases} \quad (18)$$

For such a combination of signal and reference, the calculation of $g_n(\tau)$, as outlined in Appendix B, yields

$$\begin{aligned} & g_n(\tau_0 + p t_b) \\ &= \frac{1}{M} \sum_{m=1}^M b_m \exp \left[j 2\pi (m-1) \frac{n}{M} \right] \\ & \left\{ \begin{aligned} & \frac{\tau_0}{t_b} \frac{\sin \frac{\pi n \tau_0}{T}}{\frac{\pi n \tau_0}{T}} \exp \left[j \left(\phi_{M+m-p-1} - \phi_m + \frac{\pi n \tau_0}{T} \right) \right] \\ & + \left(1 - \frac{\tau_0}{t_b} \right) \frac{\sin \frac{\pi n (t_b - \tau_0)}{T}}{\frac{\pi n (t_b - \tau_0)}{T}} \\ & \times \exp \left[j \left(\phi_{M+m-p} - \phi_m + \frac{\pi n (t_b + \tau_0)}{T} \right) \right] \end{aligned} \right\} \quad (19) \end{aligned}$$

where $0 \leq \tau_0 < t_b$ and $p = 0, 1, 2, \dots$. Note that a negative delay can be described by its complement to T , since

$$g_n(-\tau) = g_n(T - \tau). \quad (20)$$

VI. P3 AND P4 POLYPHASE CODES

These codes, suggested by Lewis and Kretschmer [5], are basically phase samples of a linear-FM signal. The phase sequence of a P4 signal can be described by

$$\phi_m = \frac{\pi}{M} (m-1)^2 - \pi(m-1), \quad m = 1, 2, \dots, M \quad (21)$$

and of the P3 signal by

$$\phi_m = \frac{\pi}{M} (m-1)^2, \quad m = 1, 2, \dots, M; \quad M \text{ even.} \quad (22)$$

In addition to the property of perfect periodic autocorrelation, these signals exhibit a unique feature. When a phase staircase is added, which results in an accumulation of 2π over one sequence, the new code is a one bit shift of the original code (plus a constant phase). Using (21) note for P4 that

$$\phi_m + \frac{2\pi}{M} (m-1) = \phi_{m+1} + \pi \left(1 - \frac{1}{M} \right). \quad (23)$$

A similar result is obtained for a P3 signal.

Cross-correlation between a conjugate of the original signal and the signal with the added phase staircase, results in a one bit shift of the perfect periodic autocorrelation. A phase staircase which accumulates $2\pi n$ phase shift over one sequence, results in a shift of n bits of the autocorrelation function.

Doppler shift creates a *phase ramp* rather than a phase staircase. The ramp means that there is also a linear phase shift within each bit. For $\nu = n/T$ the result is still a sidelobe-free, n -bits shifted autocorrelation. However, as n increases, the ideal triangular form of the cross-correlation within the n th bit, is increasingly modified. This is demonstrated in Fig. 2 which is a plot of $|g_n(\tau)|$ for $n = -1, 0, 1, \dots, M-1$. Fig. 2 applies to a P4 signal with $M = 16$. Fig. 2 falsely hints about an intrabit symmetry, because it shows that

$$|g_n(n t_b + \tau_0)| = |g_n(n t_b - \tau_0)|, \quad |\tau_0| < t_b. \quad (24)$$

The symmetry, however holds only for the absolute value and not for $g_n(\tau)$ itself.

One conclusion from the unique property of $g_n(\tau)$ for P3 and P4 signals, is the need to extend the sum in (11) to $|n| > M/2$. For example, at $\tau = T/2$ the receiver response is controlled by the $n = \pm M/2$ ridges. There are no closer ridges that overshadow those two distant ridges.

Fig. 3 is a 3-D plot of the response (as given in (11)), of a Hann weighted receiver, to a P4 signal with $N = M = 16$. The vertical scale is linear (voltage unit). Note how on a linear scale the sidelobes in both delay and Doppler are invisible, except for the first few Doppler sidelobes near each one of the main peaks. The four peaks in Fig. 3 correspond to the points $(0, 0)$, $(T, 0)$, $(t_b, 1/T)$ and $(T + t_b, 1/T)$.

We must resort to a log scale in order to demonstrate the actual sidelobe structure. Fig. 4 displays three Doppler cuts corresponding to the delays $\tau = 0, t_b$ and $2t_b$. Note how the sidelobes near the delay axis ($\nu = 0$) decrease as τ increases. The decrease of sidelobes with τ is typical of P3 and P4 signals. It stems from the fact that at $\tau = n t_b$ the function $W(\nu)$ is centered at $\nu = \pm n/T$, and near $\tau = T/2$ only distant (hence very low) sidelobes effect the vicinity of $\nu = 0$. Beyond the midpoint ($\tau = T/2$) the sidelobe level builds up due to the contributions from negative Doppler ridges. To further demonstrate that point, Fig. 5 is a delay cut at $\nu = 1/2NT$. Note the decrease of the response, with a minimum at $\tau = T/2$.

VII. STAIRCASE WEIGHT

In practice the smooth weight function given in (11) is replaced by a staircase function. Two practical values of the stair duration t_s are the bit duration ($t_s = t_b$), or the sequence duration ($t_s = T$). If more than one sample per bit is implemented in the receiver,

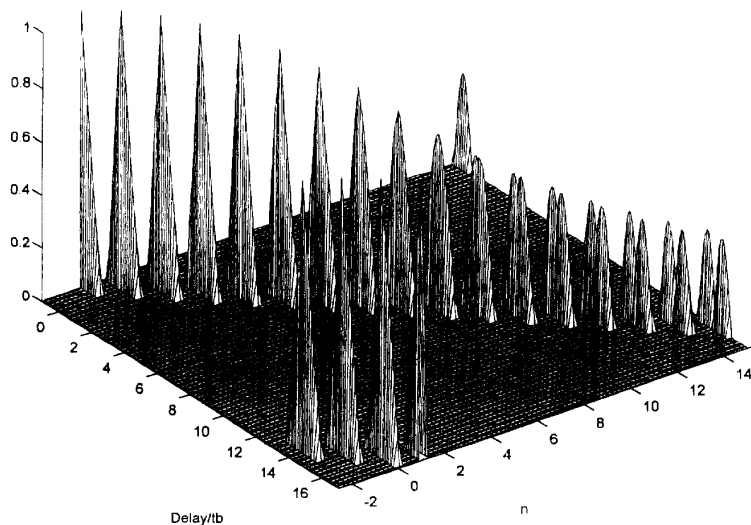


Fig. 2. $|g_n(\tau)|$ of P4 signal with $M = 16$ bits, for $n = -2$ to 15. (Artificial 3-D rendition.)

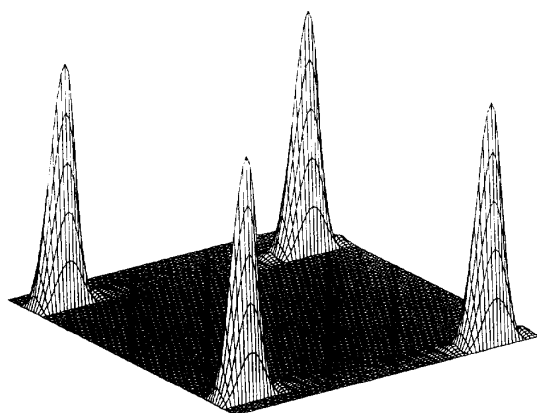


Fig. 3. Delay-Doppler response of smooth Hann weighted receiver containing $N = 16$ sequences, to P4 signal with $M = 16$ bits in a sequence. Linear (voltage) scale.

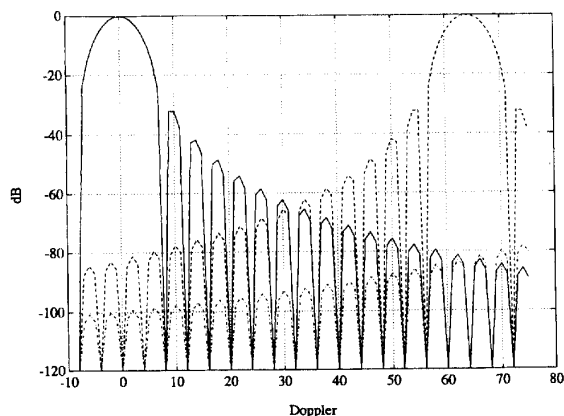


Fig. 4. Doppler cuts of response in Fig. 3 at: $\tau = 0$ (solid), $\tau = t_b$ (dash), and $\tau = 2t_b$ (dash-dot). Doppler scale unit is $1/4NT$.

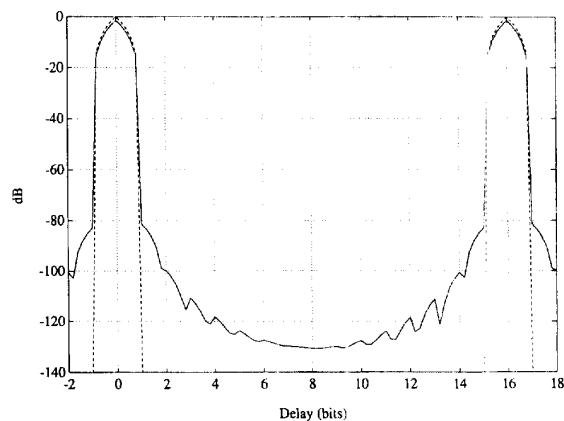


Fig. 5. Delay cuts of response in Fig. 3 at: $\nu = 0$ (dash) and $\nu = 1/2NT$ (solid).

then t_s could be even smaller than t_b . A staircase Hann weight window with $t_s = T$, is compared with a smooth Hann window in Fig. 6. Clearly, the Fourier transform $W_s(\nu)$ of the staircase window differs from the transform $W(\nu)$ of the smooth window. The Fourier transform of the staircase version of the weight window as developed in Appendix C, is

$$W_s(\nu) = \frac{\sin(\pi\nu t_s)}{\pi\nu t_s} \sum_{k=-\infty}^{\infty} (-1)^k W\left(\nu - \frac{k}{t_s}\right). \quad (25)$$

Fig. 7 presents the magnitude (in dB) of the frequency response of a staircase Hann window with $N = M = 16$. Fig. 7(a) corresponds to the case $t_s = t_b$, which means that there are $MN = 256$ stairs, while Fig. 7(b) corresponds to the case $t_s = T$, where only $N = 16$ stairs describe the weight window. The response in Fig. 7(a) is indistinguishable from the response of the truly smooth window as given in (12).

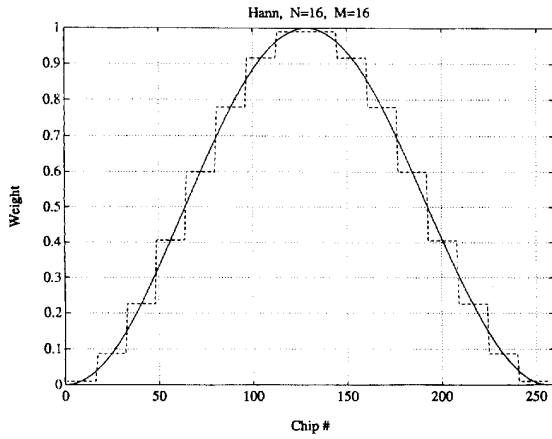


Fig. 6. Smooth and staircase Hann weight function.

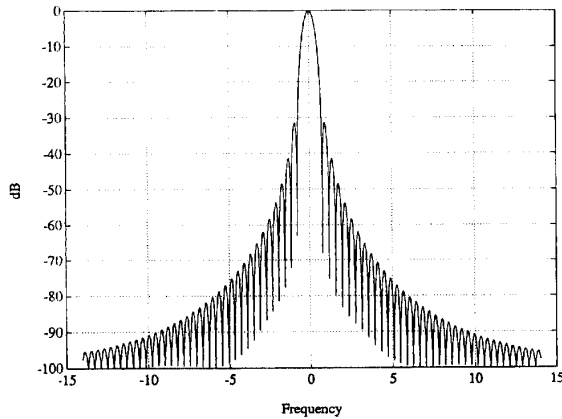


Fig. 7(a). Fourier transform of smooth Hann window.

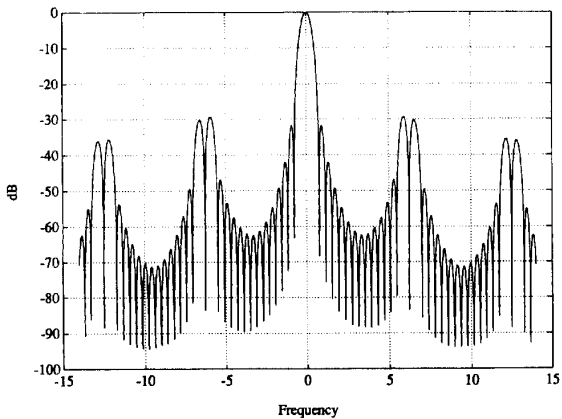


Fig. 7(b). Fourier transform of staircase Hann window with 16 stairs.

Hence from now on it is referred to as a “smooth weight window”. On the other hand, the response in Fig. 7(b) exhibits strong split-peaks at multiples of $1/t_s = 1/T$. As a matter of fact, split-peaks at multiples of $1/t_s$ exist also in the response shown in Fig. 7(a), but they are way outside the frequency scale limits.

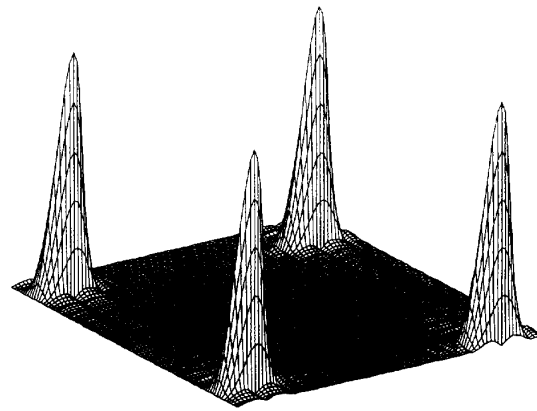


Fig. 8. Delay-Doppler response of staircase Hann weighted receiver containing $N = 16$ sequences, to P4 signal with $M = 16$ bits in a sequence. Linear (voltage) scale.

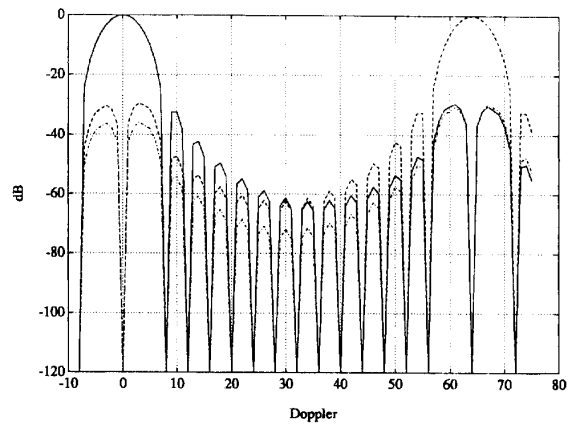


Fig. 9. Doppler cuts of response in Fig. 8 at: $\tau = 0$ (solid), $\tau = t_b$ (dash), and $\tau = 2t_b$ (dash-dot). Doppler scale unit is $1/4NT$.

Intuition may erroneously suggest that a uniform weight within each one of the N sequences of the signal will be advantageous, since it complies with the definition of autocorrelation. However, maintaining uniform weight within the sequence, implies stair-width equal to T , which results in the response shown in Fig. 7(b). The split-peaks at multiples of $1/T$ cause corresponding peaks at the receiver response. This indeed is demonstrated in the 3-D response shown in Fig. 8, in the Doppler cuts shown in Fig. 9, and in the delay cuts given in Fig. 10. These three figures correspond to a correlation receiver matched to a P4 signal with $M = N = 16$, and with staircase Hann weight, in which $t_s = T$.

Comparing the response of a receiver using a smooth Hann weight window (Figs. 3–5) with that of a staircase Hann weight (Figs. 8–10), demonstrates that the staircase Hann caused two major sidelobe ridges on the two sides of, and parallel to, the delay axis. The ridges highest cuts are at $\nu = \pm 1/NT$.

What can explain the fact that ideal autocorrelation was maintained (at $\nu = 0$) despite the use of the smooth window, which affects a nonuniform weight within each sequence? An intuitive explanation is the symmetry of the weight function. Each symmetrically located pair of sequences (e.g., the first and the last) is multiplied by symmetrical (hence inverted) slopes of the weight function. The combined weight along each pair of symmetrical sequences would have been an exact constant if the slope of the weight function, would remain constant for the duration of the sequence (T). The slope during T indeed approaches a constant as N increases.

Before moving to the next signal we wish to point out that the response for a P3 signal is similar (but not identical) to the response for the P4 signal, presented in Figs. 3–10.

VIII. TWO-VALUED SEQUENCES

Two-valued phase-coded signals with perfect periodic autocorrelation were discussed in [4, 5], and their PAF in [1]. These signals are related to the maximum-length linear shift register sequences, also known as pseudonoise (PN) sequences. However, in order to obtain the ideal (zero delay sidelobes) periodic autocorrelation, the two phase values, which constitute the alphabet of the sequence, are not 180° apart, but $\phi = \arccos[(1 - M)/(1 + M)]$ apart.

The $g_n(\tau)$ functions of these signals for $n \neq 0$, calculated using (19), have a shape of a ridge, rather than the shape of a peak, found in the P3 and P4 polyphase signals. This property was also observed [10] in PN sequences. There is no two-valued sequence of length $M = 16$, hence we discuss the nearest available code of length $M = 15$. The complex envelope of the code is given by the sequence

$$1111\beta\beta\beta1\beta\beta\beta11\beta1\beta, \quad \text{where } \beta = \exp[j \cos^{-1}(-7/8)].$$

Fig. 11 presents the $|g_n(\tau)|$ functions of this signal, for $n = -1, 0, 1, 2$. Fig. 11, as well as Fig. 2, represent an ideal delay-Doppler response, unattainable because they require infinite N . With the help of a good weight function, the near-zero Doppler-sidelobe aspect of the ideal response can be approached despite a finite N .

The response of a receiver matched to N sequences, and using a weight function, will also contain ridges at $\nu = n/T$. The sidelobe levels near $\nu = 0$ are dominated by the two nearest ridges, namely the ridges at $\nu = \pm 1/T$. Fig. 12 is a 3-D plot of the response for $N = 16$, and a "smooth" Hann weight. Fig. 13 presents the Doppler cuts at $\tau = 0$, and at $\tau = 2t_b$, using a log scale. Fig. 14 compares the delay cut at $\nu = 1/2NT$ (solid) with the ideal cut at $\nu = 0$ (dashed). These last two figures demonstrate that the random-like shape of the ridge at $\nu = 1/T$, is reproduced, attenuated by about 80 dB, at $\nu = 1/2NT$.

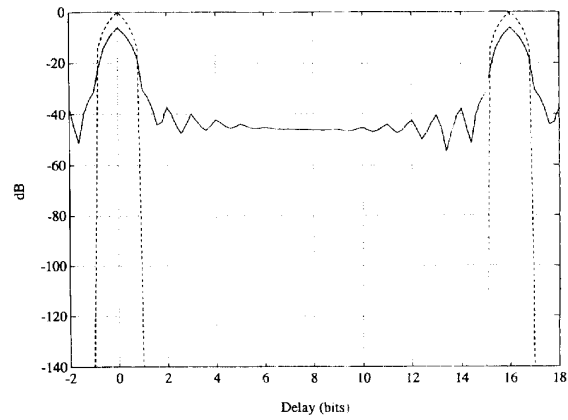


Fig. 10. Delay cuts of response in Fig. 8 at $\nu = 0$ (dash) and $\nu = 1/NT$ (solid).

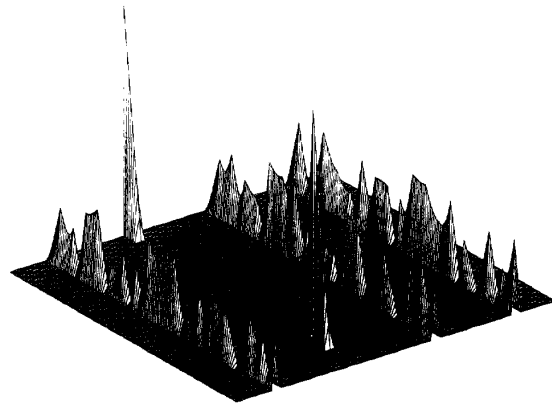


Fig. 11. $|g_n(\tau)|$ of two-valued phase-coded signal with $M = 15$ bits, for $n = -1$ to 2. (Artificial 3-D rendition.)

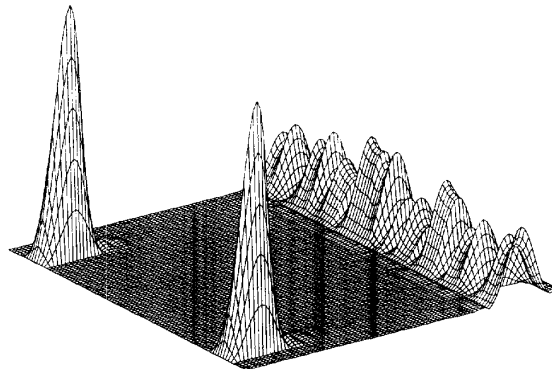


Fig. 12. Delay-Doppler response of smooth Hann weighted receiver containing $N = 16$ sequences, to two-valued phase-coded signal with $M = 15$ bits in a sequence. Linear (voltage) scale.

IX. UNMATCHED SEQUENCES

Allowing signal-to-noise (SNR) loss, it is possible to find for any length M , pairs of periodic signals

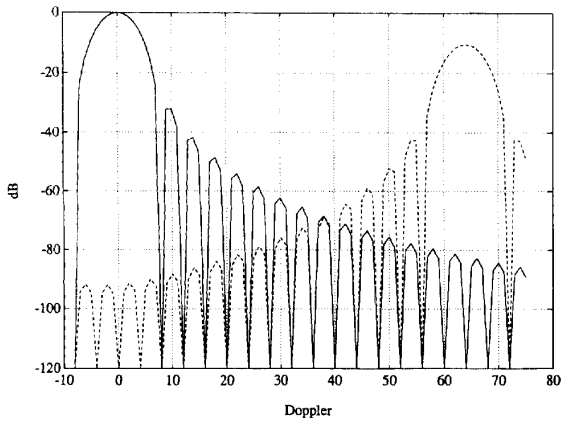


Fig. 13. Doppler cuts of response in Fig. 12 at: $\tau = 0$ (solid) and $\tau = 2t_b$ (dash).

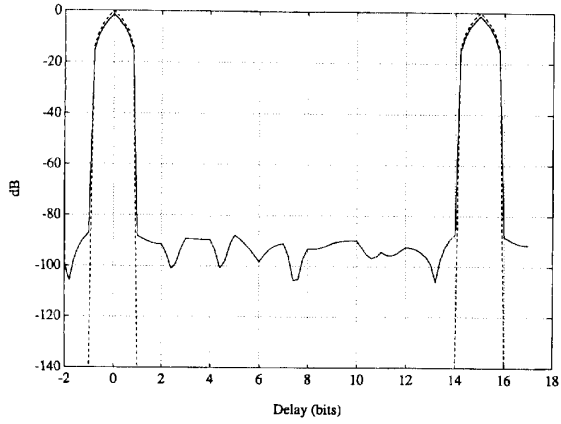


Fig. 14. Delay cuts of response in Fig. 12 at: $\nu = 0$ (dash) and $\nu = 1/2NT$ (solid).

with perfect periodic cross-correlation, in which the complex envelope of the transmitted signal uses a real two-valued alphabet (+1 and -1), while the reference signal is multivalued, but also real [11].

Of special interest are pairs which combine low loss and a small alphabet reference signal (possibly two-valued). Ipatov and Fedorov [6] presented construction algorithms for such signals.

As an example for such a signal we use the signal of length $M = 40$. The construction can be implemented using a ternary shift register as demonstrated in Fig. 15. The reference signal in the receiver is obtained by replacing each -1 in the transmitted signal with $-b$. For the $M = 40$ signal $b = 9/5$. In other words, in (18) when $\phi_m = 0$ then $b_m = 1$ and when $\phi_m = \pi$ then $b_m = 9/5$. For this particular signal the SNR loss due to the mismatch is only 0.37 dB. Using a nonuniform weight window in the receiver adds its inherent loss.

Fig. 16 presents the $|g_n(\tau)|$ function, calculated using (19), of Ipatov's code of length $M = 40$, for $n =$

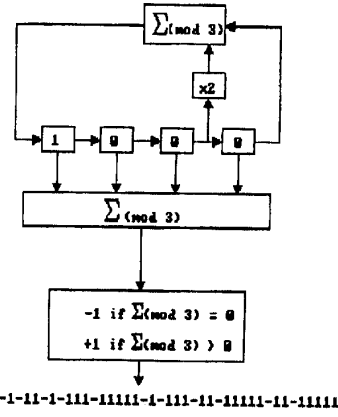


Fig. 15. Generation of Ipatov's code of length $M = 40$, using a ternary shift register.

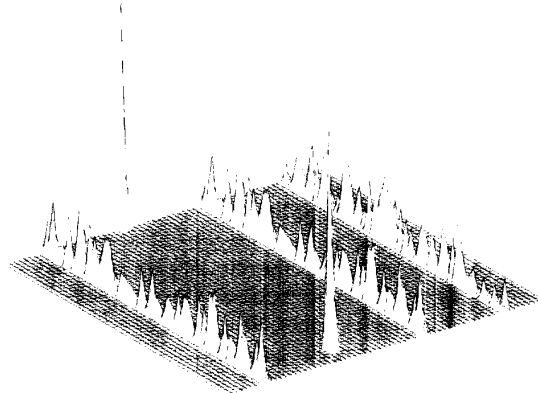


Fig. 16. $|g_n(\tau)|$ of Ipatov's signal with $M = 40$ bits, for $n = -1$ to 2. (Artificial 3-D rendition.)

-1, 0, 1, and 2. The function exhibits ridges similar to those found in the matched two-valued signal discussed in the preceding section. Two differences however can be observed. (1) There are no nulls of $|g_n(\tau)|$ at $\tau = mT$ for $m = 0, \pm 1, \pm 2, \dots$ and $n = \pm 1, \pm 2, \dots$. Such nulls appeared in the two other cases (Figs. 2 and 11) and must appear [1] in any *matched* response, when the reference signal is the complex conjugate of the transmitted signal. (2) Because the phase alphabet is constructed from 0° and 180° there must exist

$$|g_n(\tau)| = |g_{-n}(\tau)|. \quad (26)$$

Indeed, Fig. 16 demonstrates that $|g_{-1}(\tau)| = |g_1(\tau)|$. That was not the case in Figs. 2 and 11. A detailed response of a weighted receiver to Ipatov's signal is not presented because of the similarity to the response obtained with the matched two-valued sequences.

X. CONCLUSIONS

Our paper has extended the analytical tools for studying the expected theoretical delay-Doppler

response of CW radar signals. The use of the PAF was extended to account for a mismatched receiver. The term mismatched covers both weight functions and a modified reference signal. Short of the effects of hardware imperfections, this work provides formulas for calculating the delay-Doppler response of any phase-coded CW radar.

Using these tools on several phase-coded signals, revealed that, contrary to intuition, in order to reduce Doppler sidelobes, a smooth rather than a staircase weight function should be preferred. They also enabled us to demonstrate that a combination of a signal with perfect periodic autocorrelation, a large number (N) of periods in the reference signal, and a smooth weight function, can create a response with extremely low delay and Doppler sidelobes. Low sidelobes are critical toward extending the range of CW radars, where the weak target return must compete with the ever present, strong close-in clutter, entering through those sidelobes.

All the theoretical results presented here were confirmed by numerical simulation of ideal correlation receivers (not described here). Regarding the response of an actual receiver (implemented in hardware), it should agree with theory, if the receiver will not have gross imperfections and if linearity will be maintained over a large dynamic range. The next extension of these tools will try to incorporate into the analysis the effects of hardware imperfections. Ongoing work has already shown, for example, that of all the CW signals considered here, Ipatov's signals suffer the least from imbalance in the I and Q detector.

A note added at proof: In a paper by Ipatov which came to our attention recently (V. P. Ipatov et al., Boundaries of the sidelobes of a periodic discrete signal in a broad Doppler band, *Radio Engineering and Electronic Physics*, **29** (Feb. 1984), 25-32) it is pointed out that the complex envelopes of the transmitted and reference signals obey (using our terminology)

$$\begin{aligned} & \sum_{m=0}^{M-1} \left| \sum_{k=0}^{M-1} u_{k+m} r_k^* \exp\left(-j2\pi \frac{kn}{M}\right) \right|^2 \\ &= \sum_{m=0}^{M-1} \left[\left(\sum_{p=0}^{M-1} u_{p+m} u_p^* \right) \left(\sum_{q=0}^{M-1} r_{q+m} r_q^* \right) \right]^* \\ & \quad \times \exp\left(-j2\pi \frac{mn}{M}\right). \end{aligned}$$

Applying this result to signals with ideal (zero sidelobes) $g_0(\tau)$, it can be shown that in such signals

$$\sum_{m=0}^{M-1} |g_n(mt_b)|^2 = |g_0(0)|^2 \left(\frac{\sin \frac{n\pi}{M}}{\frac{n\pi}{M}} \right)^2.$$

This property can be noticed qualitatively in Figs. 2, 11 and 16.

APPENDIX A. FOURIER TRANSFORM OF $u(t-\tau)r(t)$

This Appendix develops the results in (8) and (9). We wish to develop the expression

$$\psi_\infty(\tau, \nu) = \int_{-\infty}^{\infty} u(t-\tau)r(t) \exp(j2\pi\nu\tau) dt. \quad (27)$$

We break the integral into a sum of integrals

$$\psi_\infty(\tau, \nu) = \sum_{k=-\infty}^{\infty} \left[\int_{0+kT}^{T+kT} u(t-\tau)r(t) \exp(j2\pi\nu\tau) dt \right]. \quad (28)$$

Since both $u(t-\tau)$ and $r(t)$ are periodic with period T , we can write

$$\begin{aligned} & \psi_\infty(\tau, \nu) \\ &= \int_0^T \left\{ u(t-\tau)r(t) \sum_{k=-\infty}^{\infty} \exp[j2\pi\nu(t+kT)] \right\} dt \end{aligned} \quad (29)$$

which can be split into a product of two expressions

$$\begin{aligned} \psi_\infty(\tau, \nu) &= \frac{1}{T} \int_0^T u(t-\tau)r(t) \exp(j2\pi\nu\tau) dt \\ & \quad \cdot T \sum_{k=-\infty}^{\infty} \exp(j2\pi\nu kT). \end{aligned} \quad (30)$$

One of several methods to convert the infinite sum of exponents into an infinite sum of delta functions, is to use the Poisson summation formula, whose general form is

$$\sum_{n=-\infty}^{\infty} F(n) = \sum_{k=-\infty}^{\infty} \left[\int_{-\infty}^{\infty} F(x) \exp(j2\pi kx) dx \right]. \quad (31)$$

We can fit it to our purpose by choosing

$$F(x) = \delta\left(\nu - \frac{x}{T}\right). \quad (32)$$

Using (32) in the integral of (31) and changing the variable to

$$y = \frac{x}{T}; \quad dx = T dy \quad (33)$$

yields

$$\begin{aligned} & \int_{-\infty}^{\infty} \delta\left(\nu - \frac{x}{T}\right) \exp(j2\pi kx) dx \\ &= T \int_{-\infty}^{\infty} \delta(\nu - y) \exp(j2\pi kyT) dy \\ &= T \exp(j2\pi k\nu T). \end{aligned} \quad (34)$$

Using (32) in the left-hand side of (31) and using (34) in the right-hand side of (31) yields

$$\sum_{n=-\infty}^{\infty} \delta\left(\nu - \frac{n}{T}\right) = T \sum_{k=-\infty}^{\infty} \exp(j2\pi k\nu T). \quad (35)$$

Using (35) in (30) yields

$$\psi_{\infty}(\tau, \nu) = \frac{1}{T} \int_0^T u(t-\tau)r(t) \exp(j2\pi\nu\tau) dt \cdot \sum_{n=-\infty}^{\infty} \delta\left(\nu - \frac{n}{T}\right) \quad (36)$$

which can also be written as

$$\psi_{\infty}(\tau, \nu) = \sum_{n=-\infty}^{\infty} \left[\delta\left(\nu - \frac{n}{T}\right) \frac{1}{T} \int_0^T u(t-\tau)r(t) \times \exp\left(j2\pi\frac{n}{T}t\right) dt \right]. \quad (37)$$

APPENDIX B. $g_n(\tau)$ OF PHASE-CODED SIGNALS

This Appendix outlines the calculation of $g_n(\tau)$ as defined in (9) and repeated below

$$g_n(\tau) \equiv \frac{1}{T} \int_0^T u(t-\tau)r(t) \exp\left(\frac{j2\pi n\tau}{T}\right) dt \quad (38)$$

for a periodically modulated phase-coded signal, in which a modulation period is constructed of M bits of duration t_b each, whose complex envelope is described by the sequence

$$u_m(t) = \begin{cases} \exp(j\phi_m), & 0 \leq t \leq t_b; \\ 0, & \text{elsewhere;} \end{cases} \quad m = 1, 2, \dots, M \quad (39)$$

and the reference envelope is described by the sequence

$$r_m(t) = \begin{cases} b_m \exp(-j\phi_m), & 0 \leq t \leq t_b; \\ 0, & \text{elsewhere;} \end{cases} \quad m = 1, 2, \dots, M. \quad (40)$$

The delay τ can be described by

$$\tau = \tau_0 + pt_b \quad (41)$$

where $0 \leq \tau < t_b$ and p is an integer. With the help of Fig. 17 we note that the integral in (38) can be written as a sum of M integrals,

$$g_n(\tau) = \frac{1}{T} \sum_{m=1}^M I_m = \frac{1}{Mt_b} \sum_{m=1}^M I_m \quad (42)$$

where

$$I_1 = \int_0^{\tau_0} r_1 u_{M-p} \exp\left(j2\pi\frac{n}{T}t\right) dt + \int_{\tau_0}^{t_b} r_1 u_{M-p+1} \exp\left(j2\pi\frac{n}{T}t\right) dt \quad (43)$$

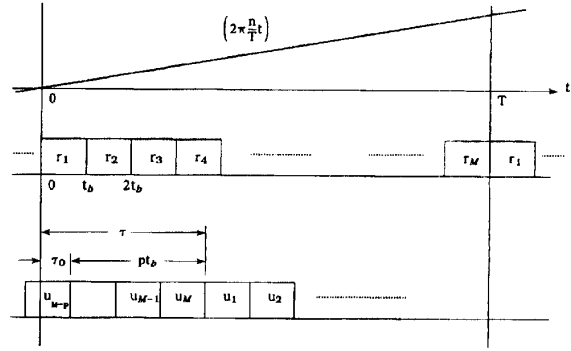


Fig. 17. Alignment of received and reference signals and Doppler phase ramp.

and correspondingly

$$I_m = \int_{(m-1)t_b}^{(m-1)t_b + \tau_0} r_m u_{M-p+m-1} \exp\left(j2\pi\frac{n}{T}t\right) dt + \int_{(m-1)t_b + \tau_0}^{mt_b} r_m u_{M-p+m} \exp\left(j2\pi\frac{n}{T}t\right) dt. \quad (44)$$

Using (39) and (40) we can rewrite (44) as

$$I_m = b_m \exp[j(\phi_{M-p+m-1} - \phi_m)] \times \int_{(m-1)t_b}^{(m-1)t_b + \tau_0} \exp\left(j2\pi\frac{n}{T}t\right) dt + b_m \exp[j(\phi_{M-p+m} - \phi_m)] \times \int_{(m-1)t_b + \tau_0}^{mt_b} \exp\left(j2\pi\frac{n}{T}t\right) dt. \quad (45)$$

Performing the integrals in (45) yields

$$I_m = t_b b_m \exp\left[j2\pi(m-1)\frac{n}{M}\right] \times \left\{ \frac{\tau_0}{t_b} \frac{\sin\frac{\pi n\tau_0}{T}}{\frac{\pi n\tau_0}{T}} \exp\left[j\left(\phi_{M+m-p-1} - \phi_m + \frac{\pi n\tau_0}{T}\right)\right] + \left(1 - \frac{\tau_0}{t_b}\right) \frac{\sin\frac{\pi n(t_b - \tau_0)}{T}}{\frac{\pi n(t_b - \tau_0)}{T}} \times \exp\left[j\left(\phi_{M+m-p} - \phi_m + \frac{\pi n(t_b + \tau_0)}{T}\right)\right] \right\}. \quad (46)$$

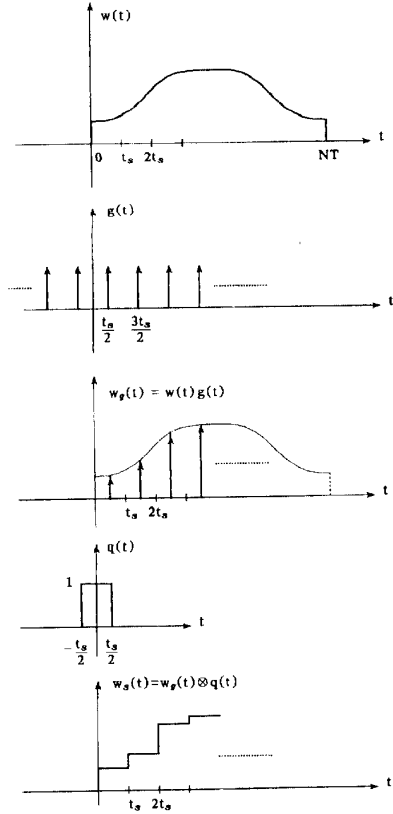


Fig. 18. Mathematical construction of staircase weight function.

Using (46) in (42) yields the final result

$$g_n(\tau_0 + pt_b) = \frac{1}{M} \sum_{m=1}^M b_m \exp \left[j2\pi(m-1) \frac{n}{M} \right] \cdot \left\{ \frac{\tau_0}{t_b} \frac{\sin \frac{\pi n \tau_0}{T}}{\frac{\pi n \tau_0}{T}} \exp \left[j \left(\phi_{M+m-p-1} - \phi_m + \frac{\pi n \tau_0}{T} \right) \right] + \left(1 - \frac{\tau_0}{t_b} \right) \frac{\sin \frac{\pi n (t_b - \tau_0)}{T}}{\frac{\pi n (t_b - \tau_0)}{T}} \times \exp \left[j \left(\phi_{M+m-p} - \phi_m + \frac{\pi n (t_b + \tau_0)}{T} \right) \right] \right\}. \quad (47)$$

APPENDIX C. STAIRCASE WEIGHT WINDOW

The Fourier transform of a staircase weight window is obtained. Fig. 18 demonstrates how the window is constructed. The smooth window $w(t)$ extends from $t = 0$ to $t = NT$. Its Fourier transform is $W(\nu)$. The steps are of duration t_s , with the first step centered at $t_s/2$, and receiving the value $w(t_s/2)$, and so on. We assume that NT/t_s is an integer.

The staircase window is generated by first multiplying the smooth weight window $w(t)$ by a train

of impulses shifted from the origin by $t_s/2$

$$g(t) = \sum_{k=-\infty}^{\infty} \delta \left(t - kt_s - \frac{t_s}{2} \right). \quad (48)$$

The Fourier transform of $g(t)$ is $G(\nu)$

$$G(\nu) = \frac{1}{t_s} \sum_{k=-\infty}^{\infty} (-1)^k \delta \left(\nu - \frac{k}{t_s} \right). \quad (49)$$

The resulting sampled waveform is

$$w_g(t) = w(t)g(t) \quad (50)$$

whose transform is

$$W_G(\nu) = W(\nu) \otimes G(\nu) = \frac{1}{t_s} \sum_{k=-\infty}^{\infty} (-1)^k W \left(\nu - \frac{k}{t_s} \right). \quad (51)$$

The step will be defined by the rectangular function $q(t)$, also shown in Fig. 18. Its transform is

$$Q(\nu) = t_s \frac{\sin(\pi \nu t_s)}{\pi \nu t_s}. \quad (52)$$

The staircase window is obtained by convolving $w_g(t)$ with $q(t)$

$$w_s(t) = w_g(t) \otimes q(t). \quad (53)$$

The Fourier transform of the staircase window is therefore

$$W_S(\nu) = W_G(\nu)Q(\nu) = \frac{\sin(\pi \nu t_s)}{\pi \nu t_s} \sum_{k=-\infty}^{\infty} (-1)^k W \left(\nu - \frac{k}{t_s} \right). \quad (54)$$

REFERENCES

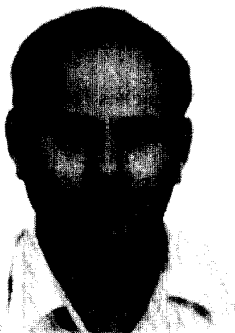
- [1] Levanon, N., and Freedman, A. (1992) Periodic ambiguity function of CW signals with perfect periodic autocorrelation. *IEEE Transactions on Aerospace and Electronic Systems*, **28**, 2 (Apr. 1992), 387-395.
- [2] Levanon, N. (1993) CW alternatives to the coherent pulse train—signals and processors. *IEEE Transactions on Aerospace and Electronic Systems*, **29**, 1 (Jan. 1993), 250-254.
- [3] Kretschmer, F. E., and Lewis, B. L. (1983) Doppler properties of polyphase coded pulse compression waveforms. *IEEE Transactions on Aerospace and Electronic Systems*, **AES-19**, 4 (July 1983), 521-531.
- [4] Bomer, L., and Antweiler, M. (1990) Binary and biphasic sequences and arrays with low periodic autocorrelation sidelobes. In *Proceedings of the International Conference on Acoustics, Speech, and Signal Processing*, Albuquerque, NM, 1990, 1663-1666.
- [5] Golomb, S. W. (1992) Two-valued sequences with perfect periodic autocorrelation. *IEEE Transactions on Aerospace and Electronic Systems*, **28**, 2 (Apr. 1992), 383-386.

- [6] Ipatov, V. P., and Fedorov, B. V. (1984)
Regular binary sequences with small losses in suppressing sidelobes.
Radioelectronic and Communication Systems, 27, 3 (Mar. 1984), 29–33.
- [7] Freedman, A., and Levanon, N. (1994)
Properties of the periodic ambiguity function.
IEEE Transactions on Aerospace and Electronic Systems, 30, 3 (July 1994), 938–941.
- [8] Rihaczek, A. W. (1969)
Principles of High Resolution Radar.
New York: McGraw-Hill, 1969.
- [9] Nuttall, A. H. (1981)
Some windows with very good sidelobe behavior.
IEEE Transactions on Acoustics, Speech and Signal Processing, 29, 1 (Feb. 1981), 84–91.
- [10] Persons, C. E. (1966)
Ambiguity function of pseudo-random sequences.
Proceedings of the IEEE, 54, 12 (Dec. 1966), 1946–1947.
- [11] Rohling, H., and Plagge, W. (1989)
Mismatched-filter design for periodical binary phased signals.
IEEE Transactions on Aerospace and Electronic Systems, 25, 6 (Nov. 1989), 890–897.



Benjamin J. Getz was born in Tel-Aviv, Israel, in 1967. He received his B.Sc. degree in physics and mathematics, cum laude, in 1988 from the Hebrew University in Jerusalem, and the M.Sc. degree in electrical engineering from Tel-Aviv University, summa cum laude, in 1994.

From 1985 to 1993 he served in the Israeli Air Force. Since 1994 he is employed by Elisra Ltd.



Nadav Levanon (S'67—M'69—SM'83) was born in Israel in 1940. He received the B.Sc. and M.Sc. in electrical engineering from the Technion-Israel Institute of Technology, Haifa, in 1961 and 1965, respectively, and the Ph.D. in electrical engineering from the University of Wisconsin, Madison, in 1969.

From 1961 to 1965 he served in the Israeli Army. He has been a faculty member at Tel-Aviv University since 1970, first in the Department of Geophysics, and since 1977 in the Department of Electronic Systems, where he is a Professor. He was Chairman of that department from 1983 to 1985. He was a Visiting Associate Professor at the University of Wisconsin, from 1972 to 1974, and a Visiting Scientist at The Johns Hopkins University, Applied Physics Laboratory, in the academic year 1982–1983.

He is the author of the book *Radar Principles* (Wiley, 1988).